INTERNATIONAL JOURNAL OF HYDROGEN ENERGY XXX (XXXX) XXX

Available online at www.sciencedirect.com

ScienceDirect

journal homepage: www.elsevier.com/locate/he

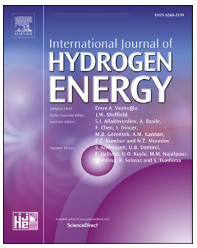

Tuning an ionic-electronic mixed conductor $NdBa_{0.5}Sr_{0.5}Co_{1.5}Fe_{0.5}O_{5+\delta}$ for electrolyte functions of advanced fuel cells

Nabeela Akbar, Sara Paydar, Yan Wu *

Engineering Research Center of Nano-Geo Materials of Ministry of Education, Faculty of Materials Science and Chemistry, China University of Geosciences, 388 Lumo Road, Wuhan, 430074, PR China

HIGHLIGHTS

- A mixed ionic electronic conductor NBSCF was tuned as an electrolyte via BZCY.
- The 10 wt% BZCY effectively suppressed the electronic conductivity of NBSCF.
- BZCY–NBSCF cell exhibited an enhanced ionic conductivity of 0.16 S cm^{-1} at 550 °C.
- BZCY–NBSCF cell showed a power density of 470 mW cm^{-2} at 550 °C.
- The interfacial conduction could take a crucial role in the ion transporting process.

ARTICLE INFO

Article history:
Received 11 December 2019
Received in revised form
11 May 2020
Accepted 20 May 2020
Available online xxx

Keywords:
$NdBa_{0.5}Sr_{0.5}Co_{1.5}Fe_{0.5}O_{5+\delta}$ (NBSCF)
Semiconductor/ionic composite
Ionic conductivity
Advanced fuel cell

ABSTRACT

An ionic-conducting electrolyte mainly governs the solid oxide fuel cell performance. In this work, a mixed conductor $NdBa_{0.5}Sr_{0.5}Co_{1.5}Fe_{0.5}O_{5+\delta}$ was tuned as an electrolyte via compositing with a proton conductor $BaZr_{0.3}Ce_{0.6}Y_{0.1}O_{3-\delta}$ (BZCY), which realizes an ionic conductivity of 0.16 S cm^{-1} at 550 °C along with fuel cell power density of 470 mW cm^{-2}. The 10 wt.% proton conducting BZCY can not only effectively block the electronic conductivity of NBSCF, but also greatly improve its ionic conductivity and the corresponding device's power output. The interfacial conduction could take a crucial role in the ion transporting process of BZCY-NBSCF composite. These interfaces or nanoscale grain boundaries formed amongst two phases keep excellent capability for designing and creating high performance electrochemical devices along with high-power density.

Introduction

Solid oxide fuel cells (SOFCs) desire a swift ion transportation in electrodes and electrolytes to rapid up fuel cell efficiency for the beneficial power outputs and long term durability [1–6]. Nowadays, the exploration for electrolyte materials with higher ionic conductivity in the low temperature range (less than 600 °C) is a main step towards dropping the operation temperature of fuel cells, which is currently above 700 °C, as conventional SOFC using yttrium stabilized zirconia (YSZ) used for electrolyte necessitates operates at high temperature i.e. 800-1000 °C to obtain an enough ionic conductivity, which results in high expenses and lack of commercialization

* *Corresponding author.*
E-mail address: wuyan@cug.edu.cn (Y. Wu).

https://doi.org/10.1016/j.ijhydene.2020.05.220

viability [7–12]. Proton conducting materials, because of lower activation energy than O^{2-} conduction, high ionic conductivity and theoretical electrical efficiency in the targeted low temperature range, are favorable materials for electrolyte in SOFCs [13]. Recently a composite membrane consisting of semiconductor NCAL ($Ni_{0.8}Co_{0.15}Al_{0.05}LiO_{2-\delta}$) and ($Ce_{0.8}Sm_{0.2}O_{2-\delta}$ -Na_2CO_3) as electrolyte, was reported to act as the electrolyte layer in a new fuel cell technology and exhibited significantly upgraded performance as compared to conventional fuel cell [14]. For example, the heterostructure formation between the mixed ionic electronic conductor (MIEC) $BaCo_{0.4}Fe_{0.4}Zr_{0.1}Y_{0.1}O_{3-\delta}$ and a semiconductor ZnO can significantly attain super ionic conductivity and high cell performance at 500 °C [2].

Amongst the semiconductor materials, the layered perovskite oxide materials have drawn much attention as favorable cathode materials for low temperature solid oxide fuel cells (LTSOFCs) because of their significantly fast oxygen reduced reaction kinetics and high electrical conductivities [15–18]. These Layered perovskite oxides keep a typical formula of $AA'B_2O_{5+\delta}$, in which A can be a trivalent lanthanide ion (Nd, Sm, Pr, Gd and Pr); A′ can be Sr or Ba, and B can be the first row transition metal element (B =Mn, Cu, Fe, Co, Ni, etc.) [19]. Consequently, a beneficial channel is created through the AO_δ layer, by the mean of which oxygen ion diffusivity enhances due to the reduced oxygen bonding energy, through the lanthanide layer [20,21]. Due to the fast oxygen kinetics and advantageous electrochemical properties Co rich layered perovskites i.e. $LnBaCo_2O_{5+\delta}$, also have garnered extensive consideration in this field [15,16]. Recently, cation-ordered double-perovskite structures such as NBSCF as an electrode has attracted much attention due to its easier oxygen ion diffusion, faster surface oxygen exchange and higher electrical conductivity at lower temperatures than simple perovskite cathode materials. In addition, it displayed excellent stabilities and compatibility with the proton-conducting electrolyte [22–26]. Besides the fact that, Cobalt rich layered perovskites usually show bad long-term fuel cell stability performance. Hence, numerous ion exchange effects are being considered in efforts to improve their stability and performance [17].

Particularly, between the considered cathodes, Fe and Sr co-doped double perovskite oxides show exceptional electrochemical performance, long-term stability and electrical conductivity outputs [19]. On the other side, among the discovered proton-conducting oxides used as electrolytes, $BaCe_{1\_x}Zr_xY_{0.1}O_{2.95}$ ($0 < x < 1$) materials are reported as the most favorable candidates for proton conducting SOFC applications because of their fast proton movement and relatively high conductivity [27–29]. In this study, we further develop the promising triple-conducting NBSCF composited with $BaZr_{0.1}Ce_{0.7}Y_{0.2}O_{3-\delta}$ used as an electrolyte for LTSOFCs. We investigated its properties from two aspects: 1) ionic conductivity in electrolyte process; 2) electrochemical properties, to improve and develop advanced LTSOFCs. The observed performances and measured results suggest excellent ionic conductivity in the BZCY-NBSCF composite membrane, which tends to insight semiconductor/ionic composite perspectives to design advanced electrolytes for LTSOFC with high performance.

Experimental

Materials synthesis

All the chemical agents were purchased from Sinopharm chemical reagent co. LTD, including Nd $(NO_3)_3 \cdot 6H_2O$, Sr $(NO_3)_2$, Co $(NO_3)_2 \cdot 6H_2O$, Ba $(NO_3)_2$, Fe $(NO_3)_3 \cdot 6H_2O$, citric acid and ethylene glycol. NBSCF ($NdBa_{0.5}Sr_{0.5}Co_{1.5}Fe_{0.5}O_{5+\delta}$) was synthesized by using the Pichini method. Proper amounts of Nd $(NO_3)_3 \cdot 6H_2O$, Ba $(NO_3)_2$, Sr $(NO_3)_2$, Co $(NO_3)_2 \cdot 6H_2O$ and Fe $(NO_3)_3 \cdot 6H_2O$ were added and dissolved in distilled water with appropriate amounts of citric acid and ethylene glycol to prepare a gel. The prepared solution was heated and combusted to get required powder, and then calcinated at 600 °C for 4 h to obtain pure phase NBSCF. Material for electrolyte -functional layers was synthesized by using an altered Pechini process. The as-prepared NBSCF and Ba, Zr, Ce, and Y metal nitrates were dissolved in distilled water (the designed weight ratio between added NBSCF and BZCY was 9:1) and citric acid was added as a reacting agent. The solution was stirred and heated at 70 °C for 2 h. The composition was supposed to be Ba $(Zr_{0.1}Ce_{0.7}Y_{0.2})$ $O_{3-\delta}$. Ethylene glycol (Aldrich, 99%) as a polymerization agent was added to the solution. The attained solution was heated at 250 °C for 4 h, and a dark grey-black colored ash was found. Finally, the resulting ash was successively calcined at 1000 °C for 3 h to yield BZCY-NBSCF composition powder.

Fuel cell fabrication

The configuration of fabricated fuel Cells was Ni-NCAL ($Ni_{0.8}Co_{0.15}Al_{0.05}LiO_2$)/BZCY-NBSCF/NCAL-Ni, where the BZCY-NBSCF composite was pressed in the middle of two Ni-NCAL round foams. The cell was assembled by one step pressing under a load of 200 MPa to make a symmetrical cell having thickness of 1 mm and diameter of 13 mm with an active area of 0.64 cm^2. The NCAL powder was purchased from Tianjin Bamo Science &Technology Joint Stock Ltd., China. Then a slurry was prepared by mixing the NCAL powder with terpineol and ethanol, which was brushed on one side of nickel foam (1.5 mm thick, 98% porosity); finally, the Ni-NCAL coating was kept at 60 °C for 2 h to remove the terpineol and ethanol. The resulting NCAL-pasted Ni foam (NCAL-Ni) was obtained for electrodes together with the current collector. A symmetrical fuel cell was fabricated using the homogeneous layer of BZCY-NBSCF compacted between two pieces of NCAL-Ni electrodes under 200 MPa uniaxial load for 10 s into one pellet. The fabrication of two fuel cells was in symmetrical configuration of NCAL-Ni/NBSCF/NCAL-Ni and NCAL-Ni/BZCY-NBSCF/NCAL-Ni respectively. Before tests, the fuel cells were kept at 550 °C for 1 h, then the fuel cell performance was measured with hydrogen as fuel and air as oxidant at atmospheric pressure in a hydrogen flow of 100 ml min^{-1} and air flow of 110 ml min^{-1} respectively.

Material characterizations

The X-ray diffraction (XRD) characterization of the samples was carried out by using a Bruker D8–FOCUS X-ray

Please cite this article as: Akbar N et al., Tuning an ionic-electronic mixed conductor $NdBa_{0.5}Sr_{0.5}Co_{1.5}Fe_{0.5}O_{5+\delta}$ for electrolyte functions of advanced fuel cells, International Journal of Hydrogen Energy, https://doi.org/10.1016/j.ijhydene.2020.05.220

diffractometer (Germany) to identify the phases of NBSCF and composite samples. The sample morphologies and microstructures were examined by a Tecnai G2 F30 transmission electron microscope (TEM, FEI, USA) functioning at an acceleration voltage of 300 kV to get high resolution transmission electron microscopy (HRTEM) images and scanning electron microscopy (SEM) (SU8010, Hitachi Japan). An environmental scanning electron microscope armed with an energy dispersive X-ray spectroscope (EDX, SU8010, Hitachi, japan) was also employed for the microstructure of the samples and their chemical element investigation. Elemental composition information was clarified using X-ray photoelectron spectroscopy (XPS) investigation that was carried out by using an Escalab 250Xi (Thermo Scientific, Mass, USA). The EIS spectroscopy (electrochemical impedance spectra) were conducted by means of an electric chemical workstation (Zennium E, Zahner, Germany) between 550 °C and 490 °C. The applied frequency ranged was from 1 MHz to 0.01 Hz with a bias voltage of 10 mV. In addition, a digital instrument (ITECH8511, ITECH Electrical Co., LTD.) was applied to determine *I*–*P* (current-power) and *I*–*V* (current-voltage) characteristics.

Results and discussions

Crystalline structure and morphology

The attained XRD patterns of as-synthesized NBSCF, BZCY and BZCY-NBSCF composite are shown in Fig. 1a. The diffraction peaks of pure NBSCF and BZCY well correspond to perovskite structures without any impurities. In BZCY-NBSCF all diffraction peaks of the composite can be allocated to NBSCF and BZCY, evincing that the two phases co-existed in the composite and no objectionable reaction happened during the synthesis process. The crystallite size (*d*) was calculated by the following Eq. (1).

$$d = K\lambda/(\beta \cos\theta) \quad (1)$$

here, *K* is a constant i.e. 0.9; θ, the peak position; β, peak width at half maximum intensity; λ, the wavelength of the radiation, respectively. The calculated average crystallite size of the NBSCF powder is observed to be 19 nm. SEM (scanning electron microscope) and TEM (transmission electron microscope) are employed to inspect the structure and morphology of BZCY-NBSCF composite where the particles are tightly agglomerated which is revealed by SEM (in Fig. 1b). Fig. 1c provides TEM image of the composite to portray its homogeneous distribution of nanoscale particles. It is clearly seen that the contacts are produced among these particles or grains. In the typical high-resolution TEM (HRTEM) image of the BZCY-NBSCF (Fig. 1d) it can be seen that the distinct crystalline fringes having lattice spacing of 0.22 nm matches to the (112) crystalline plane of NBSCF and lattice spacing of 0.31 nm matches to the (002) crystalline plane of BZCY are also observed. Consequently, the interfaces between BZCY and NBSCF are clearly recognized, as marked in the images, and continuous interfaces are established.

The energy dispersive spectrometer (EDS) map scan at scanning transmission electron microscopy (STEM) model was performed to further identify the distribution and diffusion of elements in the interface. Fig. 2(b–k) reveal that Ba, Ce,

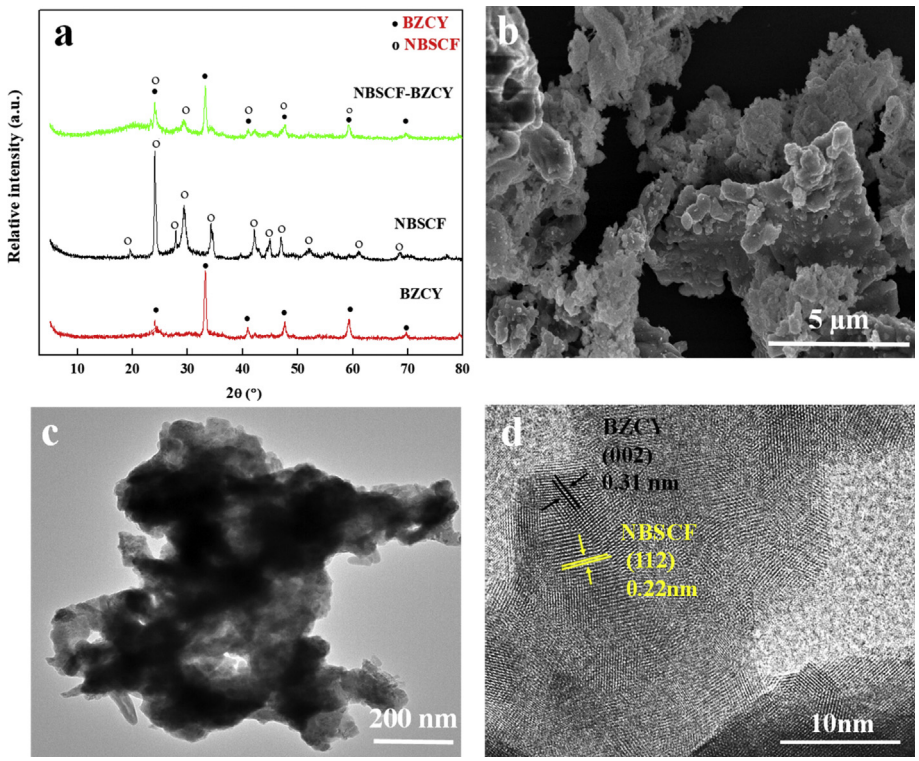

Fig. 1 – (a) XRD patterns of NBSCF, BZCY and BZCY-NBSCF composite, (b) SEM image of BZCY-NBSCF composite powder, (c) TEM image of BZCY-NBSCF composite, (d) HRTEM image of BZCY-NBSCF composite.

Please cite this article as: Akbar N et al., Tuning an ionic-electronic mixed conductor $NdBa_{0.5}Sr_{0.5}Co_{1.5}Fe_{0.5}O_{5+\delta}$ for electrolyte functions of advanced fuel cells, International Journal of Hydrogen Energy, https://doi.org/10.1016/j.ijhydene.2020.05.220

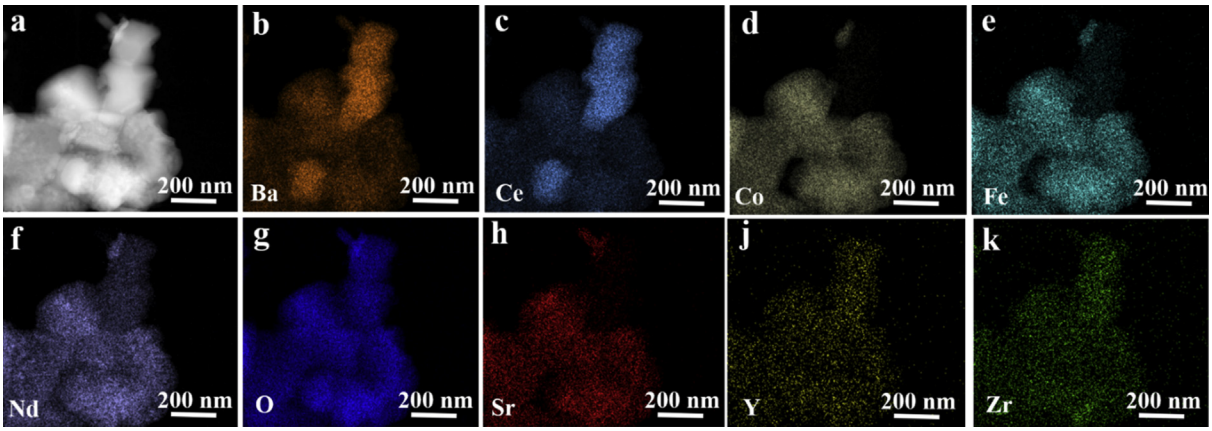

Fig. 2 – Chemical characterization of element environment change. (a) HRTEM image of BZCY-NBSCF composite particles, (b–k) The EDS mapping of HRTEM for BZCY-NBSCF composite.

Co, Fe, Nd, O, Sr, Y and Zr elements are uniformly distributed throughout the particles in the selected region.

XPS was carried out to further determine the electron state of elements of the composite. Fig. 3a presents the survey spectra of NBSCF and BZCY-NBSCF samples. Ba, Ce, Co, Fe, Nd, O, Sr, Y and Zr main elements can be observed in the sample; C element is likely remained from the surfactant during the synthesis procedure. The O 1s spectrum illustrated in Fig. 3b indicates that the oxygen element chemical environment in NBSCF and BZCY-NBSCF is significantly different, which is deduced from the divergence of peak position and shape. The O 1s spectrum is elaborately divided into lattice oxygen (O_L) and the chemical absorbed oxygen (O_C) [30,31]. The concentration of chemical absorbed oxygen is correlated with the number of oxygen vacancies which serve as defects to provide active sites for oxygen ions transport. As shown in Fig. 3b the discrepancy of the lattice oxygen's position is correlated to the divergence in the chemical environment in the material. Besides, the ratio of $Area_2$:$Area_1$ in BZCY-NBSCF is 0.32 which is larger in comparison with those of NBSCF (0.25), indicating the increase of the oxygen vacancies in BZCY-NBSCF composite. It is significant noting that the additional oxygen vacancies are advantageous for promotion on catalyst activity of materials [32].

Fuel cell performance

The current-power density (*I–P*) and current-voltage (*I–V*) characteristic tests of the electrolyte functionality of the pure phase NBSCF and the BZCY-NBSCF composite in LTSOFC, is shown in Fig. 4a. As it can be seen the devices attained the highest power density of 220 mW cm^{-2} and 470 mW cm^{-2} at 550 °C for pure NBSCF and BZCY-NBSCF composite, respectively. The results proved that the incorporation of 10% BZCY can significantly enhance the fuel cell performance. This enhancement is primarily due to the improved proton transportation in the electrolyte; Moreover, during the fuel cell operation, protons can be electrochemically injected in the NBSCF or BZCY-NBSCF electrolyte, and the proton movement can lessen the resistance at the interface of the electrolyte/electrode in the fuel cell device. Consequently, the ion conduction of H^+/O^{2-} may be a case, which is counted as a more attractive candidate for LTSOFCs, e.g. ceria-carbonate electrolyte [33]. Fig. 4b shows the power outputs of the BZCY-NBSCF fuel cell operated at different temperatures. At 550 °C the power density and voltage were found to be 470 mW cm^{-2} and 1.0 V respectively. Further gradually reducing the temperature from 550 to 490 °C, the power densities decline and the corresponding OCVs also slightly decline, but

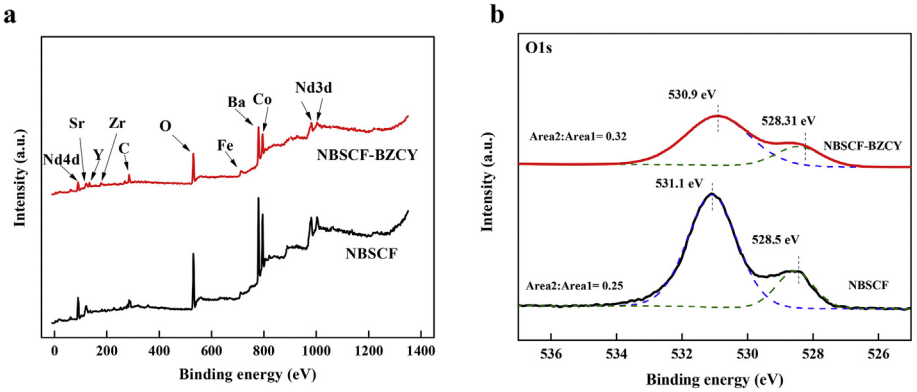

Fig. 3 – (a) XPS spectra of NBSCF and BZCY-NBSCF composite, (b) O 1s scan of NBSCF and BZCY-NBSCF samples.

Please cite this article as: Akbar N et al., Tuning an ionic-electronic mixed conductor $NdBa_{0.5}Sr_{0.5}Co_{1.5}Fe_{0.5}O_{5+\delta}$ for electrolyte functions of advanced fuel cells, International Journal of Hydrogen Energy, https://doi.org/10.1016/j.ijhydene.2020.05.220

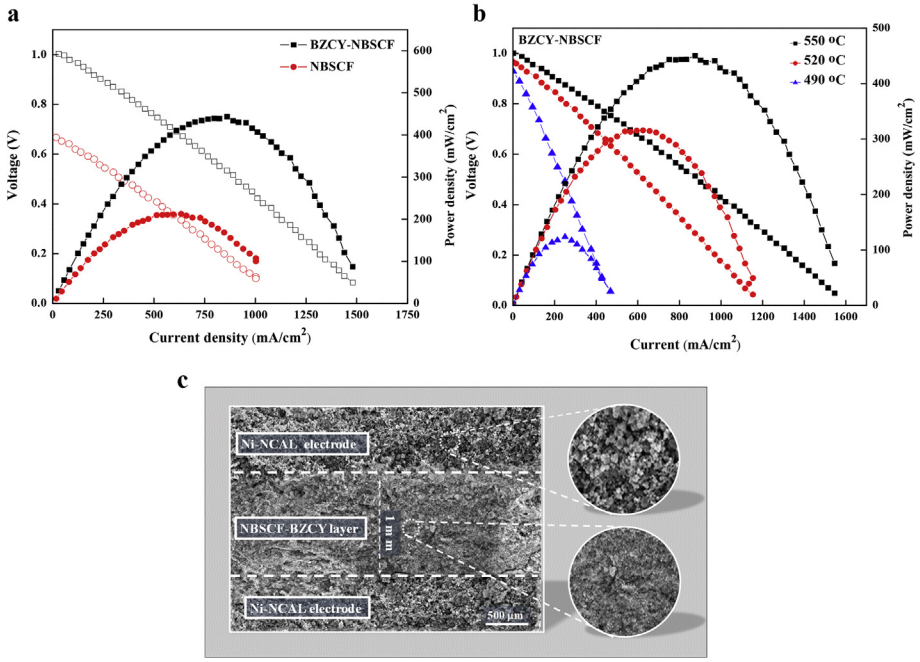

Fig. 4 – (a) Comparing the *I*–*V* and *I*–*P* curve of fuel cell based on pure NBSCF and BZCY-NBSCF composite, (b) *I*–*V* and *I*–*P* curve of fuel cell based on BZCY-NBSCF composite at different temperature, (c) cross-section SEM image of the fuel cell with BZCY-NBSCF composite electrolyte after fuel cell operation at 550 °C with the magnified view.

100 mW cm^{-2} and above 0.9 V can be reached at 490 °C to indicate good LTSOFC performances. However, the SEM cross-section image of the cell with BZCY-NBSCF electrolyte after fuel cell operation is given in Fig. 4c, where the three layers of relatively dense electrolyte, porous cathode and anode are shown.

Electrochemical and electrical conductivity analysis

The underlying conductivity change at the pure NBSCF and BZCY-NBSCF composite is represented by electrochemical impedance spectra (EIS) in Fig. 5. It is obvious from Fig. 5 that at 550 °C the ohm resistance values (R_o) of cells having pure NBSCF and BZCY-NBSCF composite as electrolytes are 0.44 Ω cm^2 and 0.185 Ω cm^2, respectively. Fig. 5b exhibits the representative EIS of BZCY-NBSCF fuel cell tested in H_2/air at 490, 520, and 550 °C under open-circuit conditions. These EIS data are fitted with an equivalent circuit of R_o (R_1Q_1) (R_2Q_2) (Fig. 5b), and all the simulated resistivities are summed up in Table 1. In this equivalent circuit, at high frequencies the intercept on the real axis (Z') empirically relate to R_o and on the other hand the R_1Q_1 and R_2Q_2 represent the grain boundary behavior at intermediate frequency and electrode polarization process of electrode at low frequency, respectively [2,34]. It principally originates from the resistance of electrolyte layer, counting the electronic and ionic resistances, which was found to be 0.185, 0.28 and 0.32 Ω cm^2 at 550, 520 and 490 °C, respectively for the BZCY-NBSCF composite. Besides, small grain-boundary resistances indicate the high conductivity of BZCY-NBSCF at 490–550 °C, which could be attributed to the advent of the high ionic conductive phase significantly reducing the grain boundary resistances of the composite by introducing BCZY proton conductor. To study the effect of proton injection on the fuel cell performance, we analyzed the EIS results before and after proton injection i.e. in air/air atmosphere and H_2/air atmosphere respectively, where we observed that the conductivity experienced a transition from very low intrinsic electronic conduction of 2.6×10^{-4} S cm^{-1} of BZCY-NBSCF nanocomposite in air (Fig. 5c) to a colossal conduction transition above 3 orders of magnitude to reach 0.16 S cm^{-1} in fuel cell environment at 550 °C (as shown in Fig. 5b).

Fig. 6a shows that the temperature dependence for ionic conductivity of the BZCY-NBSCF sample. By considering the simulated R_0 and R_1 at various temperatures, the total conductivity (σ_t) of BZCY-NBSCF is calculated. Additionally, the ionic resistance of BZCY-NBSCF can be attained using the slope of the linear part in the measured *I*–*V* curves (Fig. 4b), as that the linear part in the middle region mirrors ohmic polarization which is mainly related to the resistance of ion transportation in the electrolyte [35]. Therefore, the ionic conductivity of BZCY-NBSCF was obtained to be 0.16 S cm^{-1} at 550 °C. The activation energy (E_a) was calculated from the following Eq. (2):

$$\sigma = A \exp\left(-\frac{E_a}{kT}\right) \quad (2)$$

where σ corresponds to conductivity; A is pre-exponent factor; k is donating Boltzmann constant; T is representing absolute temperature. Fig. 6b shows the temperature dependence for total conductivities of the BZCY-NBSCF composite. From which, we can extricate the activation energy (E_a) of BZCY-NBSCF composite is 0.45 eV at a temperature range of 550 to 490 °C. These results reveals that by introducing a proton

Please cite this article as: Akbar N et al., Tuning an ionic-electronic mixed conductor $NdBa_{0.5}Sr_{0.5}Co_{1.5}Fe_{0.5}O_{5+\delta}$ for electrolyte functions of advanced fuel cells, International Journal of Hydrogen Energy, https://doi.org/10.1016/j.ijhydene.2020.05.220

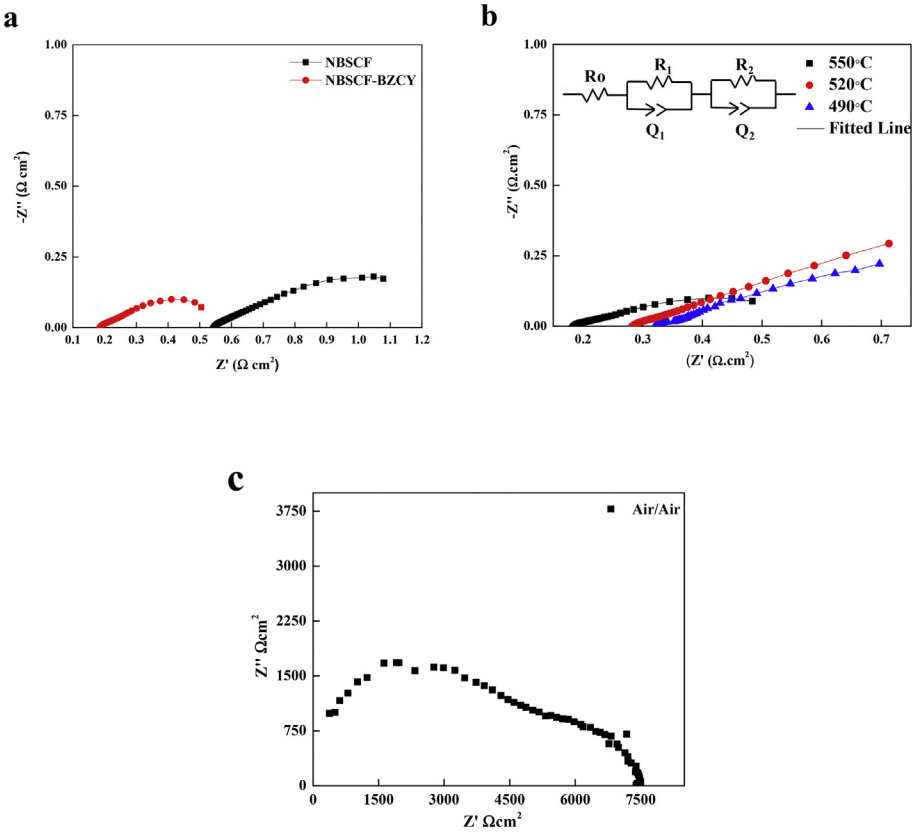

Fig. 5 – Impedance spectra of (a) pure NBSCF and BZCY-NBSCF composite with NCAL electrodes operating at 550 °C, (b) BZCY-NBSCF composite fuel cell with NCAL electrodes at different temperatures in H_2/air conditions, (c) BZCY-NBSCF composite fuel cell under air/air atmosphere before fuel cell operation at 550 °C.

Table 1 – Equivalent circuit analysis results of EIS of the cell based on BZCY-NBSCF composite at 550-490 °C in H_2/air condition.

Temperature (°C)	R_0 (Ω cm^2)	R_1 (Ω cm^2)	R_2 (Ω cm^2)
550	0.185	0.045	0.372
520	0.28	0.0457	0.92
490	0.32	0.05	0.98

conductor (10 wt.%) can effectively enhance ionic conductivity along with the mobile ion concentration, by exhibiting a low activation energy for ion transportation and giving rise to a better fuel cell performance, which suggests that the designed composite with BZCY has an interesting mechanism of ion transportation which deserves for continuous study in future work.

Based on above results, the ionic conductivity of NBSCF has been significantly enhanced by compositing with BZCY. Consequently, the interfacial conduction could take a crucial role in studying the ion transport mechanism in BZCY-NBSCF composite, as in the interface region (Fig. 7), the defect concentrations are much higher than that in the bulk, thus the interface supplies high conductivity pathways for ionic

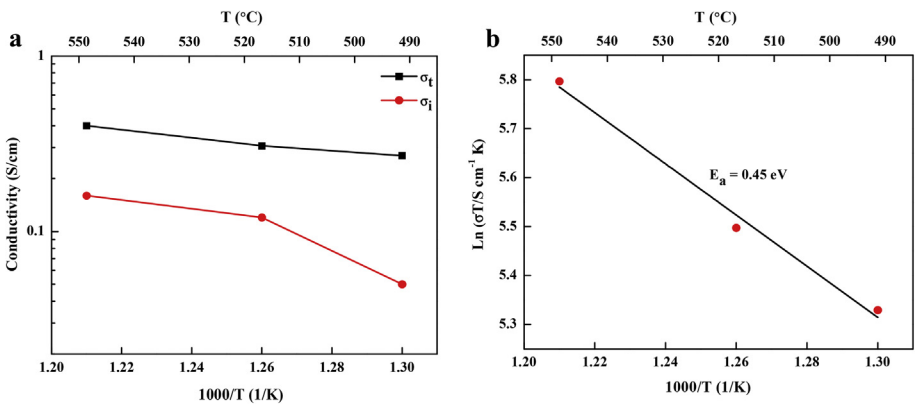

Fig. 6 – Total and ionic conductivities of BZCY-NBSCF as a function of 1000/T at 490–550 °C.

Please cite this article as: Akbar N et al., Tuning an ionic-electronic mixed conductor $NdBa_{0.5}Sr_{0.5}Co_{1.5}Fe_{0.5}O_{5+\delta}$ for electrolyte functions of advanced fuel cells, International Journal of Hydrogen Energy, https://doi.org/10.1016/j.ijhydene.2020.05.220

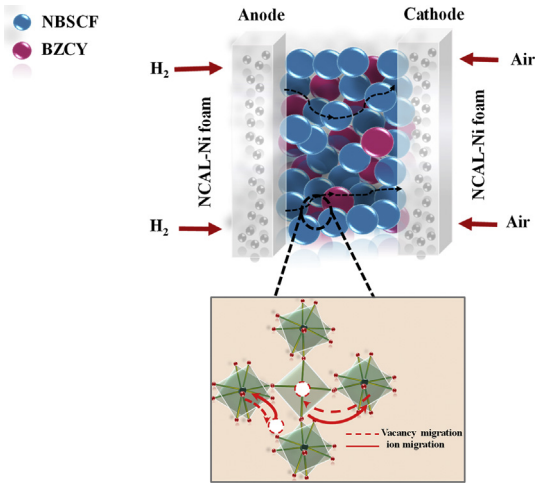

Fig. 7 – Ion transport mechanism of BZCY-NBSCF.

transportation and conduction. In addition, the created interfaces and nanoscale grain boundaries between two phases have great capacity for designing and manufacturing electrochemical devices with high efficiency and high-power output. Especially in nanocomposite, this interfacial effect is dominant in overall ionic transport. This can explain the greatly enhanced conductivity of BZCY-NBSCF composite compared to the single phase NBSCF electrolyte [36–38]. The nano-composite BZCY-NBSCF undeniably exhibits high potential on the way to energy conversion: As NBSCF is a triple ionic conductor, and BZCY has dominant proton conduction and electron blocking ability, the intersection of these two phases at the nano-scale may generate excessive defects (oxygen vacancies/surface oxygen-ions) i.e. interfaces, as a result the overall electronic conduction of the material suppresses giving raise to the enhanced ionic conductivity and the cell performance [21,39]. It is also found by Tao et al. that the electron-blocking ability of the composite is highly dependent on the amount of $BaCeO_3$ and increased with increasing $BaCeO_3$ content at the grain boundary interface [40] Associated to the bulk structure, exceptional properties of nanostructured components are mainly due to a huge number of interface-defects which corresponds to the heterogenous composite [38,41].

Conclusion

We tuned NBSCF material to be ionic conducting electrolyte and further developed the high-performance BZCY-NBSCF composite electrolyte by introducing 10 wt.% BCZY proton conductors. Using BZCY to form the heterogenous composite with the NBSCF improve the fuel cell performance up to 470 mW cm^{-2} which is more than twice as compared to the pure NBSCF and the ionic conductivity reaches 0.16 S cm^{-1}. This study presents a strong indication to support the better ionic transport and fuel cell performance. This work leads a new approach to design and develop advanced materials and devices for SOFCs.

Acknowledgments

This work is supported by the National Natural Science Foundation of China (NSFC, grant No. 51774259).

REFERENCES

[1] Liu L, Li L, Yang Y, Wu Y, Zhu B. Fast ion channels for crab shell-based electrolyte fuel cells. Int J Hydrogen Energy 2019;44:15370–6. https://doi.org/10.1016/j.ijhydene.2019.04.048.

[2] Xia C, Mi Y, Wang B, Lin B, Chen G, Zhu B. Shaping triple-conducting semiconductor $BaCo_{0.4}Fe_{0.4}Zr_{0.1}Y_{0.1}O_{3-\delta}$ into an electrolyte for low-temperature solid oxide fuel cells. Nat Commun 2019;1707:10. https://doi.org/10.1038/s41467-019-09532-z.

[3] Yan W, Chen X, Wei Z, Xiang Y, Zheng YB, Jiao JL, Zhu B. Natural hematite for next generation solid oxide fuel cells. Adv Funct Mater 2016;26:938–42. https://doi.org/10.1002/adfm.201503756.

[4] Xu R, Wu Y, Wang X, Zhang J, Yang X. Enhanced ionic conductivity of yttria-stabilized ZrO_2 with natural CuFe-oxide mineral heterogeneous composite for low temperature solid oxide fuel cells. Int J Hydrogen Energy 2017;42:17495–503. https://doi.org/10.1016/j.ijhydene.2017.05.218.

[5] Li L, Zhu B, Zhang J, Yan C, Wu Y. Electrical properties of nanocube CeO_2 in advanced solid oxide fuel cells. Int J Hydrogen Energy 2018;43:12909–16. https://doi.org/10.1016/j.ijhydene.2018.05.120.

[6] Zhang J, Zhang W, Xu R, Wang X, Yang X. Electrochemical properties and catalyst functions of natural CuFe oxide mineral e LZSDC composite electrolyte. Int J Hydrogen Energy 2017;42:22185–91. https://doi.org/10.1016/j.ijhydene.2017.01.163.

[7] Singhal SC. Solid oxide fuel cells for stationary, mobile, and military applications. Solid State Ionics 2002;152–153:405–10. https://doi.org/10.1016/S0167-2738(02)00349-1.

[8] Ormerod Mark R. Solid oxide fuel cells. Chem Soc Rev 2003;32:17–28. https://doi.org/10.1039/b105764m.

[9] Wang X, Afzal M, Deng H, Dong W, Wang B, Mi Y, Xu Z, Zhang W, Feng C, Wang Z, Wu Y, Zhu B. $La_{0.1}Sr_xCa_{0.9-x}MnO_{3-\delta}$-$Sm_{0.2}Ce_{0.8}O_{1.9}$ Composite Material for novel low temperature solid oxide fuel cells. Int J Hydrogen Energy 2017;2:3–9. https://doi.org/10.1016/j.ijhydene.2017.05.158.

[10] Huang J, Xie F, Wang C, Mao Z. Development of solid oxide fuel cell materials for intermediate-to-low temperature operation. Int J Hydrogen Energy 2011;37:877–83. https://doi.org/10.1016/j.ijhydene.2011.04.030.

[11] Leonard K, Lee Y, Okuyama Y. Influence of dopant levels on the hydration properties of SZCY and BZCY proton conducting ceramics for hydrogen production. Int J Hydrogen Energy 2016;42:3926–37. https://doi.org/10.1016/j.ijhydene.2016.10.120.

[12] Zhao Y, Xia C, Jia L, Wang Z, Li H, Yu J, Li Y. Recent progress on solid oxide fuel cell: lowering temperature and utilizing non-hydrogen fuels. Int J Hydrogen Energy 2013;38:16498–517. https://doi.org/10.1016/j.ijhydene.2013.07.077.

[13] O'Hayre R, Cha S-W, Colella W, Prinz FB. Fuel cell fundamentals. New York: John Wiley and Sons, Inc.; 2009.

[14] Zhang W, Cai Y, Wang BY, Xia C, Dong WJ, Li JJ, et al. Mixed ionic-electronic conductor membrane based fuel cells by

Please cite this article as: Akbar N et al., Tuning an ionic-electronic mixed conductor $NdBa_{0.5}Sr_{0.5}Co_{1.5}Fe_{0.5}O_{5+\delta}$ for electrolyte functions of advanced fuel cells, International Journal of Hydrogen Energy, https://doi.org/10.1016/j.ijhydene.2020.05.220

incorporating semiconductor $Ni_{0.8}Co_{0.15}Al_{0.05}LiO_{2-\delta}$ into the $Ce_{0.8}Sm_{0.2}O_{2-\delta}$ -Na_2CO_3 electrolyte. Int J Hydrogen Energy 2016;41:15346–53. https://doi.org/10.1016/j.ijhydene.2016.07.032.

[15] Kim G, Wang S, Jacobson AJ, Reimus L, Brodersen Pg, Mims CA. Rapid oxygen ion diffusion and surface exchange kinetics in $PrBaCo_2O_{5+x}$ with a perovskite related structure and ordered A cations. J Mater Chem 2007;17:2500–5. https://doi.org/10.1039/b618345j.

[16] Yoo S, Jun A, Ju YW, Odkhuu D, Hyodo JJ, Jeong HY, Park N, Shin J, Ishihara T, Kim G. Development of double-perovskite compounds as cathode materials for low-temperature solid oxide fuel cells. Angew Chem 2014;126:13280–3. https://doi.org/10.1002/ange.201407006.

[17] Jun A, Yoo S, Ju YW, Hyodo JJ, Choi S, Jeong HY, et al. Correlation between fast oxygen kinetics and enhanced performance in Fe doped layered perovskite cathode for solid oxide fuel cells. J Mater Chem 2015;3:15082–90. https://doi.org/10.1039/C5TA02158H.

[18] Taranco A, Skinner SJ, Chater RJ, Herna F. Layered perovskites as promising cathodes for intermediate temperature solid oxide fuel cells. J Mater Chem 2007;17:3175–81. https://doi.org/10.1039/b704320a.

[19] Kim J, Shin J, Jeong HY, Choi Y, Kim G, Liu M. Highly efficient and robust cathode materials for low-temperature solid oxide fuel cells: PrBa0.5Sr0.5Co2-xFexO5-δ. Sci Rep 2013;2426:3. https://doi.org/10.1038/srep02426.

[20] Taskin AA, Lavrov AN, Ando Y, Taskin AA, Lavrov AN, Ando Y. Achieving fast oxygen diffusion in perovskites by cation ordering. Appl Phys Lett 2005;91910:86. https://doi.org/10.1063/1.1864244.

[21] Yoo S, Choi S, Kim J, Shin J, Kim G. Investigation of layered perovskite type $NdBa_{1-x}Sr_xCo_2O_{5+\delta}$ (x = 0, 0.25, 0.5,0.75, and 1.0) cathodes for intermediate-temperature solid oxide fuel cells. Electrochim Acta 2013;100:44–50. https://doi.org/10.1016/j.electacta.2013.03.041.

[22] Junyoung K, Sivaprakash S, Goeun K, Dong D, Jeeyoung S, Meilin L, Guntae K. Triple-conducting layered perovskites as cathode materials for proton-conducting solid oxide fuel cells. ChemSusChem 2014;7:2811–5. https://doi.org/10.1002/cssc.201402351.

[23] Kim NI, Afzal RA, Choi SR, Lee SW, Ahn D, Bhattacharjee S, Lee SC, Kim JH, Park JY. Highly active and durable nitrogen doped-reduced graphene oxide/double perovskite bifunctional hybrid catalysts. J Mater Chem 2017;5:13019–31. https://doi.org/10.1039/C7TA02283B.

[24] Sihyuk C, Seonyoung Y, Jiyoun K, Seonhye P, Areum J, Sivaprakash S, Junyoung K, Jeeyoung S, Hu YJ, Yong MC, Guntae K, Meilin L. Highly efficient and robust cathode materials for low-temperature solid oxide fuel cells: PrBa0.5Sr0.5Co2-xFexO5+d. Sci Rep 2013;2426:3. https://doi.org/10.1038/srep02426.

[25] Kim NI, Sa YJ, Yoo TS, Choi SR, Afzal RA, Choi T, Seo YS, Lee KS, Hwang JY, Choi WS, Joo SH, Park JY. Oxygen-deficient triple perovskites as highly active and durable bifunctional electrocatalysts for oxygen electrode reactions. Sci Adv 2018;9360:4. https://doi.org/10.1126/sciadv.aap9360.

[26] Lee TH, Park KY, Kim NI, Song SJ, Hong KH, Ahn D, Azad AK, Hwang J, Bhattacharjee S, Lee SC, Lim HT, Park JY. Robust $NdBa_{0.5}Sr_{0.5}Co_{1.5}Fe_{0.5}O_{5+d}$ cathode material and its degradation prevention operating logic for intermediate temperature solid oxide fuel cells. J Power Sources 2016;331:495–506. https://doi.org/10.1016/j.jpowsour.2016.09.080.

[27] Kreuer KD. Aspects of the formation and mobility of protonic charge carriers and the stability of perovskite-type oxides. Solid State Ionics 1999;125:285–302. https://doi.org/10.1016/S0167-2738(99)00188-5.

[28] Kreuer KD. proton-conducting oxides. Annu Rev Mater Res 2003;33:333–59. https://doi.org/10.1146/annurev.matsci.33.022802.091825.

[29] Sandrine R, Nikolaos B, Filip L, Reine W. $LaCoO_3$: promising cathode material for protonic ceramic fuel cells based on a $BaCe_{0.2}Zr_{0.7}Y_{0.1}O_{3-\delta}$ electrolyte. J Power Sources 2012;218:313–9. https://doi.org/10.1016/j.jpowsour.2012.06.098.

[30] Dupin JC, Gonbeau D, Vinatier P, Levasseur A. Systematic XPS studies of metal oxides, hydroxides and peroxides. Phys Chem Chem Phys 2000;2:1319–24. https://doi.org/10.1039/a908800h.

[31] Xu Q. Huang D ping, Chen W, Wang H, Wang BT, Yuan RZ. X-ray photoelectron spectroscopy investigation on chemical states of oxygen on surfaces of mixed electronic-ionic conducting $La_{0.6}Sr_{0.4}Co_{1-y}Fe_yO_3$ ceramics. Appl Surf Sci 2004;228:110–4. https://doi.org/10.1016/j.apsusc.2003.12.030.

[32] Ding X, Gao Z, Ding D, Zhao X, Hou H, Zhang S, Yuan G. Cation deficiency enabled fast oxygen reduction reaction for a novel SOFC cathode with promoted CO_2 tolerance. Appl Catal B Environ 2019;243:546–55. https://doi.org/10.1016/j.apcatb.2018.10.075.

[33] Hou Z, Wang X, Wang J, Zhu B. Structural studies on ceria-carbonate composite electrolytes. Key Eng Mater 2008;372:278–81. https://doi.org/10.4028/www.scientific.net/KEM.368-372.278.

[34] Shah MAKY, Naveed M, Rauf S, Xia C, Zhu B. The semiconductor $SrFe_{0.2}Ti_{0.8}O_{3-\delta}$ -ZnO heterostructure electrolyte fuel cells. Int J Hydrogen Energy 2019;44:30319–27. https://doi.org/10.1016/j.ijhydene.2019.09.145.

[35] Zhu B, Liu XR, Zhou P. Cost-effective yttrium doped ceria-based composite ceramic materials for intermediate temperature solid oxide fuel cell applications. J Mater Sci 2001;20:591–4. https://doi.org/10.1023/A:1010900829589.

[36] Lin Y, Fang S, Su D, Brinkman KS, Chen F. Enhancing grain boundary ionic conductivity in mixed ionic–electronic conductors. Nat Commun 2015;6:1–9. https://doi.org/10.1038/ncomms7824.

[37] Co S, Fe OÀ, Wang B, Wang Y, Fan L, Cai Y, Raza R, Aken PA, Wang H, Zhu B. Preparation and characterization of Sm and Ca co-doped ceria–$La_{0.6}Sr_{0.4}Co_{0.2}Fe_{0.8}O_{3-\delta}$ semiconductor–ionic composites for electrolyte-layer-free fuel cells. J Mater Chem 2016;4:15426–36. https://doi.org/10.1039/C6TA05763B.

[38] Wang X, Afzal M, Deng H, Dong W, Wang B, Mi Y, Xu Z, Zhang W, Feng Ch, Wang Z, Wu Y, Zhu B. $La_{0.1}Sr_xCa_{0.9-x}MnO_{3-\delta}$-$Sm_{0.2}Ce_{0.8}O_{1.9}$ composite material for novel low temperature solid oxide fuel cells. Int J Hydrogen Energy 2017;2(3–9):10. https://doi.org/10.1016/j.ijhydene.2017.05.158.

[39] Li B, Liu S, Liu X, Qi S, Yu J, Wang H, Su W. Electrical properties of SDC–BCY composite electrolytes for intermediate temperature solid oxide fuel cell. Int J Hydrogen Energy 2014;39:14376–80. https://doi.org/10.1016/j.ijhydene.2014.02.129.

[40] Tao H, Zhang Y, Brinkman K. Enhanced oxygen electrocatalysis in heterostructured ceria electrolytes for intermediate-temperature solid oxide fuel cells. ACS Omega 2018;3:13559–66. https://doi.org/10.1021/acsomega.8b02127.

[41] Ma Y, Singh M, Wang X, Yang F, Huang Q, Zhu B. Study on GDC-KZnAl composite electrolytes for low-temperature solid oxide fuel cells. Int J Hydrogen Energy 2014;9:5–10. https://doi.org/10.1016/j.ijhydene.2014.01.143.

Please cite this article as: Akbar N et al., Tuning an ionic-electronic mixed conductor $NdBa_{0.5}Sr_{0.5}Co_{1.5}Fe_{0.5}O_{5+\delta}$ for electrolyte functions of advanced fuel cells, International Journal of Hydrogen Energy, https://doi.org/10.1016/j.ijhydene.2020.05.220